MUC1 and Polarity Markers INADL and SCRIB Identify Salivary Ductal Cells

**D. Wu[1,2]*, P.J. Chapela[3]*, C.M.L. Barrows[1] , D.A. Harrington[1,2,3],
D.D. Carson[3], R.L. Witt[4,5], N.G. Mohyuddin[6], S. Pradhan-Bhatt[4,5],
and M.C. Farach-Carson[1,2,3]**

Abstract

Current treatments for xerostomia/dry mouth are palliative and largely ineffective. A permanent clinical resolution is being developed to correct hyposalivation using implanted hydrogel-encapsulated salivary human stem/progenitor cells (hS/PCs) to restore functional salivary components and increase salivary flow. Pluripotent epithelial cell populations derived from hS/PCs, representing a basal stem cell population in tissue, can differentiate along either secretory acinar or fluid-transporting ductal lineages. To develop tissue-engineered salivary gland replacement tissues, it is critical to reliably identify cells in tissue and as they enter these alternative lineages. The secreted protein α-amylase, the transcription factor MIST1, and aquaporin-5 are typical markers for acinar cells, and K19 is the classical ductal marker in salivary tissue. We found that early ductal progenitors derived from hS/PCs do not express K19, and thus earlier markers were needed to distinguish these cells from acinar progenitors. Salivary ductal cells express distinct polarity complex proteins that we hypothesized could serve as lineage biomarkers to distinguish ductal cells from acinar cells in differentiating hS/PC populations. Based on our studies of primary salivary tissue, both parotid and submandibular glands, and differentiating hS/PCs, we conclude that the apical marker MUC1 along with the polarity markers INADL/PATJ and SCRIB reliably can identify ductal cells in salivary glands and in ductal progenitor populations of hS/PCs being used for salivary tissue engineering. Other markers of epithelial maturation, including E-cadherin, ZO-1, and partition complex component PAR3, are present in both ductal and acinar cells, where they can serve as general markers of differentiation but not lineage markers.

Keywords: epithelial cells, glandular, tissue engineering, adult stem cells, cell differentiation, tissue regeneration

Introduction

One in 4 adults worldwide has hyposalivation-induced xerostomia (Agostini et al. 2018), reducing quality of life and leading to difficulty eating, swallowing, and speaking (Dirix et al. 2006). Hyposalivation encourages caries formation (Vissink et al. 1988). Hyposalivation occurs after radiation therapy for treatment of head and neck cancers (Schubert and Izutsu 1987) and with systemic disease (Mortazavi et al. 2014). Despite technical advances that protect normal salivary tissue during radiation treatment, compromised secretion of both protein and water components of saliva remains common (Kawamoto et al. 2018). Localized radiation selectively depletes the acinar cell population, where more resistant ductal cells persist (Sullivan et al. 2005). Current treatments fail to restore salivary flow (Pinna et al. 2015); hence, new treatments to restore salivary tissues postradiation are warranted. We are developing a biologically based, implantable salivary gland replacement tissue built from isolated and reassembled primary human stem/progenitor cells (hS/PCs) (Srinivasan et al. 2017).

Saliva originates in a polarized population of acinar cells that vectorially secrete salivary components into a complex ductal system emptying into the mouth (Martinez 1987). As saliva moves through ducts, ion exchange with the ductal epithelium creates a hypotonic product (Proctor 2016). To restore saliva production and direct flow into the mouth, acinar cells polarize to directionally secrete salivary components into

[1]Department of Diagnostic and Biomedical Sciences, Center for Craniofacial Research, University of Texas Health Science Center at Houston School of Dentistry, Houston, TX, USA
[2]Department of Bioengineering, Rice University, Houston, TX, USA
[3]Department of BioSciences, Rice University, Houston, TX, USA
[4]Department of Biological Sciences, Center for Translational Cancer Biology, University of Delaware, Newark, DE, USA
[5]Helen F. Graham Cancer Center, Christiana Care Health Systems, Newark, DE, USA
[6]Department of Clinical Otolaryngology, Houston Methodist Hospital, Houston, TX, USA

*Authors contributing equally to this article.

A supplemental appendix to this article is available online.

Corresponding Author:
M.C. Farach-Carson, Department of Diagnostic and Biomedical Sciences, Center for Craniofacial Research, University of Texas Health Science Center at Houston School of Dentistry, 1941 East Road, BBS 4220, Houston, TX 77054, USA.
Email: Mary.C.FarachCarson@uth.tmc.edu

the lumen, without leakage into the surrounding mesenchyme. A polarized ductal cell population must form that directs saliva flow unidirectionally to the oral cavity. Current understanding of epithelial polarity, largely based on ductal cell culture and invertebrate models, proposes that establishment and maintenance of polarity require 3 major protein complexes: 1) Apical/Crumbs, 2) Partition, and 3) Scribble/SCRIB (Rodriguez-Boulan and Macara 2014). The most apical complex is CRB3/Pals1/INADL (PATJ/Crumbs), which maintains the cell's apical region. The classical Partition complex is composed of PAR3/PAR6/αPKC proteins and resides in the subapical region of the cell at the tight junctions, where it maintains separation of apical and basolateral regions (i.e., serves as a partition needed for directed secretion in polarized cells). The LGL/SCRIB/DLG (Scribble) complex is the most basal, where it prevents comixing of apical and basolateral membrane components (Assemat et al. 2008).

Salivary acinar cells, whether from fluid-producing serous parotid or mucinous submandibular, differ from ductal cells in 2 substantial ways. First, they are highly secretory and produce large amounts of fluid and protein during stimulation. Second, they have a pyramidal morphology that differs considerably from cylindrical ductal cells. The pyramidal morphology provides a greater apical surface for secretion along the intercellular secretory canaliculi in the acinar lumen (Bundgaard et al. 1977; Matsuzaki et al. 2006; Masedunskas et al. 2011). In acini, tight junctions keep the apical membrane in the canaliculi from intermingling with the basal membrane (Matsuzaki et al. 2006). In ductal cells, with less apical membrane, tight junctions perform the same function but in a smaller region. The primary contribution of ductal cells is protein and ion exchange through transmembrane channels and to transport secreted saliva to the oral cavity (Mitani et al. 1989; Lee et al. 2012). These significant functional and morphological differences between acinar and ductal epithelial cells suggest that distinct polarization mechanisms establish and maintain the 2 populations and can distinguish these cell populations in differentiating hS/PCs for tissue engineering applications. We examined components of the distinct polarity complexes present in acinar and ductal epithelial cells and the luminal marker MUC1 in human salivary gland tissues. We also examined hS/PCs obtained from explants grown, expanded, and differentiated ex vivo.

Materials and Methods

Collection and Tissue Processing

Salivary tissues were resected from consented patients undergoing surgery at the Christiana Care Health System (Newark, DE) or Houston Methodist Hospital (Houston, TX) as described (Pradhan et al. 2009). Freshly dissected, deidentified parotid or submandibular salivary glands from 6 male and 7 female patients aged 22 to 81 y were used. Procedures followed approved guidelines of overseeing institutional review boards. Upon arrival, some tissue was cut into 5-mm³ cubes, flash frozen in liquid N_2, and then embedded in optimal cutting temperature (OCT) embedding compound (Sakura Finetek). Samples were stored at −80°C until sectioned. Tissue was warmed to −20°C for 30 min before sectioning using a Leica CM1850 UV cryostat.

Explant Cultures for hS/PCs

Ten patient samples were analyzed, 5 parotid and 5 submandibular. Tissue was processed and cells isolated as detailed (Wu et al. 2018). Cells, characterized previously as hS/PCs (Srinivasan et al. 2017), were cultured as needed for individual experiments.

Hydrogel Encapsulation

Encapsulation of hS/PCs used cells (3×10^6 cell/mL) seeded in HyStem hydrogel (GS311; BioTime/Ascendance Biotechnology). Hydrogels formed by mixing reconstituted thiol-modified hyaluronic acid (HA) (5.9 mM) and poly(ethylene glycol) diacrylate (1.5 mM) at a 4:1 volume ratio, then were plated on microscope glass slides fitted with presterilized arrays of 50-μL wells made from laser-cut poly(dimethylsiloxane) (PDMS; Sylgard 184; Dow Corning) sheets, as described in Wu et al. (2019). Hydrogels were removed from the mold and cultured.

Immunostaining

Salivary tissue sections were fixed in 4% (v/v) paraformaldehyde (PFA), permeabilized in 0.02% or 0.2% (v/v) Triton X-100, and blocked in filtered 3% (w/v) bovine serum albumin (BSA) or 10% goat serum in phosphate-buffered saline (1× PBS), then incubated with primary antibodies overnight in blocking solution at 4°C. Primary antibodies are described (Appendix Table 1). Samples were rinsed in PBS 3× for 5 min each at room temperature, then incubated with Alexa Fluor 488 or 568 goat anti-rabbit IgG and/or Alexa Fluor 488 or 647 goat anti-mouse at 1:1,000 (v/v) dilution (Life Technologies) overnight at 4°C. Samples then were washed 3 times in 1× PBS. The final wash included 1 μg/mL 4′,6-diamidino-2-phenylindole (DAPI) (Biotium) to stain nuclei. Samples were sealed in ProLong Gold antifade reagent (ThermoFisher Scientific, P36930) and covered. For cell imaging, hydrogels were fixed in 4% PFA for 30 min, permeabilized in 0.02% Triton X-100 for 10 min, and blocked in filtered 3% BSA in PBS for 2 h, then incubated with primary antibody overnight in blocking solution at 4°C. Samples were rinsed in PBS 3 times for 15 min each at room temperature, followed by incubation with Alexa Fluor 488 goat anti-mouse IgG and/or Alexa Fluor 568 goat anti-rabbit at a 1:400 (v/v) dilution (Life Technologies) overnight at 4°C. Samples then were washed for 15 min, 3 times in PBS. The final wash included 1 μg/mL DAPI to stain nuclei. Secondary antibody-only controls were performed to establish any nonspecific binding of fluorophore-conjugated antibodies (Appendix Fig. 1). Samples were imaged using an A1-Rsi confocal microscope and A1R/MP confocal multiphoton microscope and analyzed using NIS Elements software (Nikon Instruments).

Laser Capture Microdissection

Frozen tissue was sectioned (6–8 μm thickness) and fixed in 100% ethanol for 1 min, then dried and stored in xylene until use. Sections were air dried for 5 min prior to laser capture microdissection (LCM) that was performed using an ArcturusXT LCM (ThermoFisher Scientific) housed in the Human Tissue Acquisition and Pathology core at Baylor College of Medicine (Houston, TX). Tissue for microdissection was examined by light microscopy, and ducts and acini were marked based on morphology. Acinar cells were identified by their flat, circular structures with basally localized nuclei and ductal cells by their raised, narrowly packed cells with centrally located nuclei. A CapSure LCM cap was placed over the selected tissue samples, and captured cells were placed in TRIzol reagent (Life Technologies) and stored at −80°C for RNA extraction.
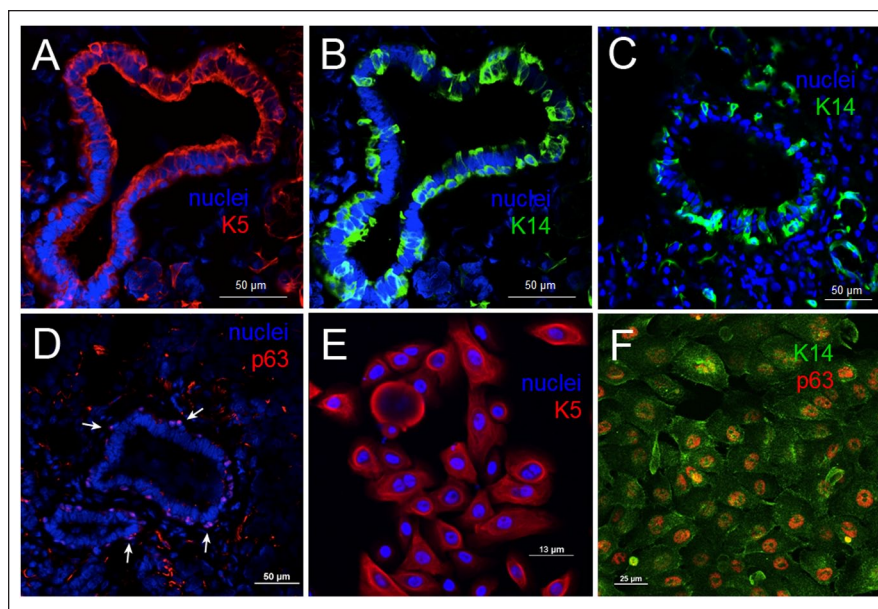
Figure 1. Tissue origin of hS/PCs. Human salivary parotid glands contain progenitor/stem cell subpopulations that express basal cell keratins K14 and K5 and stem cell marker p63 (**A–D**). These pluripotent cell populations maintain their stem/progenitor biomarkers when cultured and passaged in 2 dimensions (**E**, **F**) under nondifferentiating conditions. hS/PCs do not express ductal markers as shown in Srinivasan et al. 2017.

Extraction of RNA

RNA pellets in TRIzol were resuspended in nuclease-free water and incubated at 55°C. Remaining genomic DNA was degraded by DNaseI digest using DNA-free kit (Ambion) following the manufacturer's directions. Final RNA concentration was determined by UV absorbance using a NanoDrop 2000 spectrophotometer (ThermoFisher Scientific).

Quantitative Reverse Transcriptase Polymerase Chain Reaction

SYBR Green Supermix (Quanta Biosciences) was used for quantitative polymerase chain reaction (qPCR). Primers recognizing transcripts encoding aquaporin-5 (AQP5) (PPH16382A) were purchased from Qiagen. All other primer pairs and annealing temperatures used for reverse transcriptase polymerase chain reaction (RT-PCR) are listed in Appendix Table 2. For messenger RNA (mRNA) transcript analysis, 1 μg RNA was reverse transcribed using complementary DNA (cDNA) Supermix (Quanta Biosciences) as per the manufacturer's protocol and amplified using a Bio-Rad CFX96 Real Time System. For each 20-μL qPCR reaction, 6 μL cDNA was used.

Statistical Analyses

A 2-tailed Student's *t* test (Prism; GraphPad Software) determined statistical significance. For tissue samples, each patient was considered a biological replicate. Technical triplicates were prepared and analyzed for all qPCR samples.

Results

Isolated and Cultured Human Salivary Glands Contain Stem/Progenitor Populations Expressing K14/K5 and p63

We examined fresh-frozen human parotid tissue for basal cell keratin pair K5/14 and basal stem cell marker p63. All 3 markers were found in ducts of native parotid tissue (Fig. 1), and we identified stem/progenitor basal cell subpopulations in glands (Fig. 1A–C). Additional staining of myoepithelial cells was noted. K5/K14 staining was cytoplasmic and concentrated at cell periphery (Fig. 1A–C), whereas p63 was localized to nuclei (Fig. 1D, arrows). The cell population recognized by antibody to K5 was sizable, particularly on the luminal side, when compared to the cell subset recognized by the K14 antibody, indicating that not all cells expressed the full K5/K14 pair, also shown in Appendix Figure 2. Staining for p63 was regularly spaced in a cell subset around the duct, as typically seen for the basal cell population, in regions devoid of myoepithelial marker αSMA (Appendix Fig. 3).

The isolated hS/PC cell population expressed the same trio of markers associated with the basal cell population (Fig. 1E, F; Appendix Fig. 7), with cytokeratin staining in the cytoplasm and p63 staining in the nucleus, indicating that the hS/PC cell population is a likely isolate of the population of basal cells in tissue shown in Figure 1A–D. K14[+]/p63[+] cell populations are located in the ductal compartments (Appendix Fig. 3). Thus, the pluripotent hS/PC cells we isolate and use in tissue engineering applications possess properties of regenerative basal cells from the salivary gland that can differentiate along either
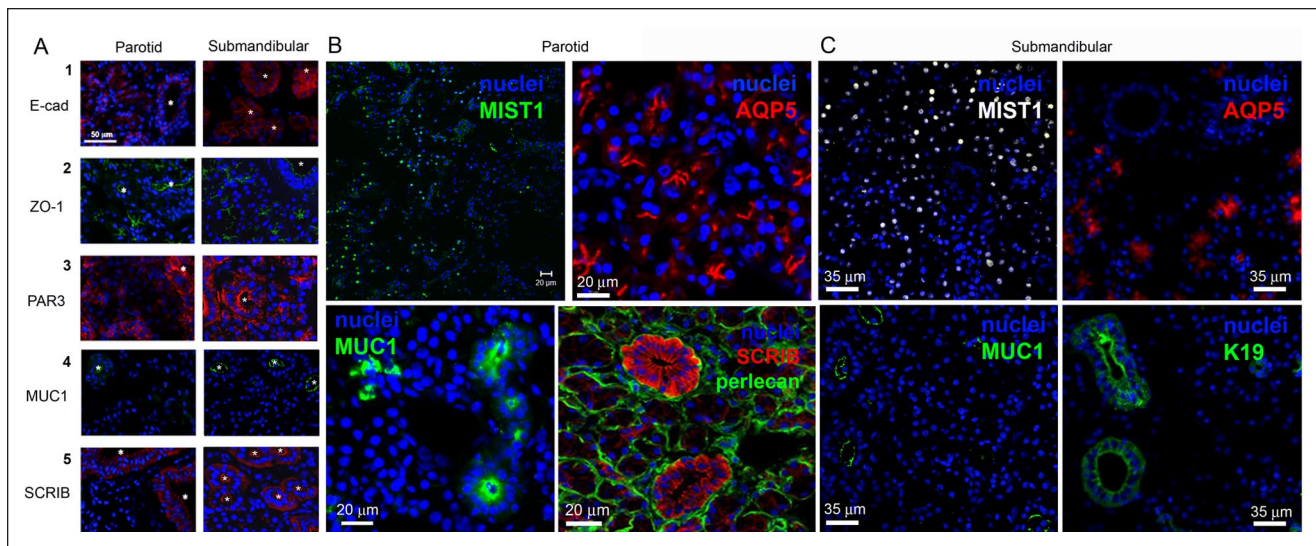
Figure 2. Tissue sections of human parotid and submandibular salivary glands. Ducts are marked with an asterisk. (**A**) Cell membranes of adherens junctions (E-cadherin [E-cad]) and tight junctions (ZO-1) are seen in both acinar and ductal epithelial cells. E-cad is present in the lateral membranes between the cells, while ZO-1 is restricted to the apical surface of the acinar cells and limited to the subapical region in ductal cells. MUC1 and SCRIB are readily visible in ductal cells but not well detected in the acini. There is strong membrane staining and weak cytoplasmic staining for PAR3, a protein found in the partition complex, for both ductal and acinar epithelial cells. Asterisks identify ductal compartments. Scale bar is 50 μm. (**B**) MIST1 staining is seen in the nuclei of acinar cells in the parotid gland. Aquaporin-5 (AQP5) staining of MIST1+ acinar regions in the parotid (red) shows the "chicken feet" pattern while no staining of ducts is seen. Staining for MUC1 (green) demarcates the luminal surface of ducts in tissue with no visible stain seen in the acinar regions. SCRIB staining in ductal cells clearly reveals the ductal population (image contributed to National Institutes of Health Image Gallery). Scale bars are 20 μm. (**C**) MIST1 staining is seen in the nuclei of acinar cells in the submandibular gland. AQP5 staining demarcates the luminal surface of the acinar cells as in the parotid without signal in the ducts. Both MUC1 and K19 clearly stain only the ductal cell populations.

acinar or ductal lineages, both needed to fully restore salivary functions.

## MUC1 and SCRIB Identify Salivary Ductal Cells

We examined expression of epithelial cell adhesion and polarity markers (Fig. 2, Appendix Figs. 4 and 6) in fresh tissue. E-cadherin was expressed at lateral interfaces of adjacent cells in both acinar and ductal (asterisks) regions (Fig. 2A1). Likewise, ZO-1 was found in both tissue regions (Fig. 2A2), but notably the staining pattern distinguished acinar structures that organized ZO-1 into a "chicken foot" along the canalicular lumen, whereas staining was circular in ductal regions. PAR3 staining was evident in both acinar and ductal tissues (Fig. 2A3, Appendix Fig. 6), particularly prominent in ductal ring-like structures near the lumen. Staining in acinar regions was more irregular, sometimes adopting the chicken foot structure. Staining of the apical epithelial MUC1 (Fig. 2A4, Appendix Fig. 4) revealed strong staining only in ductal regions nonoverlapping with αSMA. SCRIB staining was pronounced in ductal regions and was low/absent in acinar regions. As seen in Figure 2A5, ductal structures are clearly visualized by SCRIB immunostaining, with most expressing high levels of SCRIB. In another parotid gland sample (Fig. 2B, Appendix Fig. 4C, D), staining for the water channel (AQP5) in the MIST1+ acinar compartments follows the chicken foot appearance; the MUC1 staining showed rings of strong staining highlighting

ductal surfaces. Magnified images showed faint SCRIB staining of acinar cells and bright ductal "florets" encircled by the basement membrane marker perlecan/HSPG2. In submandibular gland (Fig. 2C), MIST1 and AQP5 denote the acinar compartments while K19 and MUC1 demarcate ducts present in the gland.

We failed to immunostain the polarity complex protein INADL/PATJ to assess the location of the apical complex in salivary tissues because no commercially available antibody we tested provided a selective, reliable stain without high background. Therefore, we turned to methods to detect transcripts in acinar and ductal compartments.

INADL/PATJ and MUC1 Transcripts Are Higher in Ductal Cells

Using laser capture microdissection, we separately isolated cells from acinar and ductal regions of frozen submandibular and parotid glands, 5 each (Fig. 3). Acinar cell regions contained associated myoepithelial cells. Serous parotid tissue structure was compromised by the freezing process (bottom panels visualized by U6 in situ hybridization), leading to more "compartment mixing" during laser capture (Fig. 3C). More mucinous submandibular tissue architecture held up, better allowing cleaner microdissection. Cell isolates were prepped for assessment of *INADL/PATJ* transcripts by qPCR (Fig. 3B). *MUC1* (ductal marker) and *AQ5* (acinar marker) transcripts
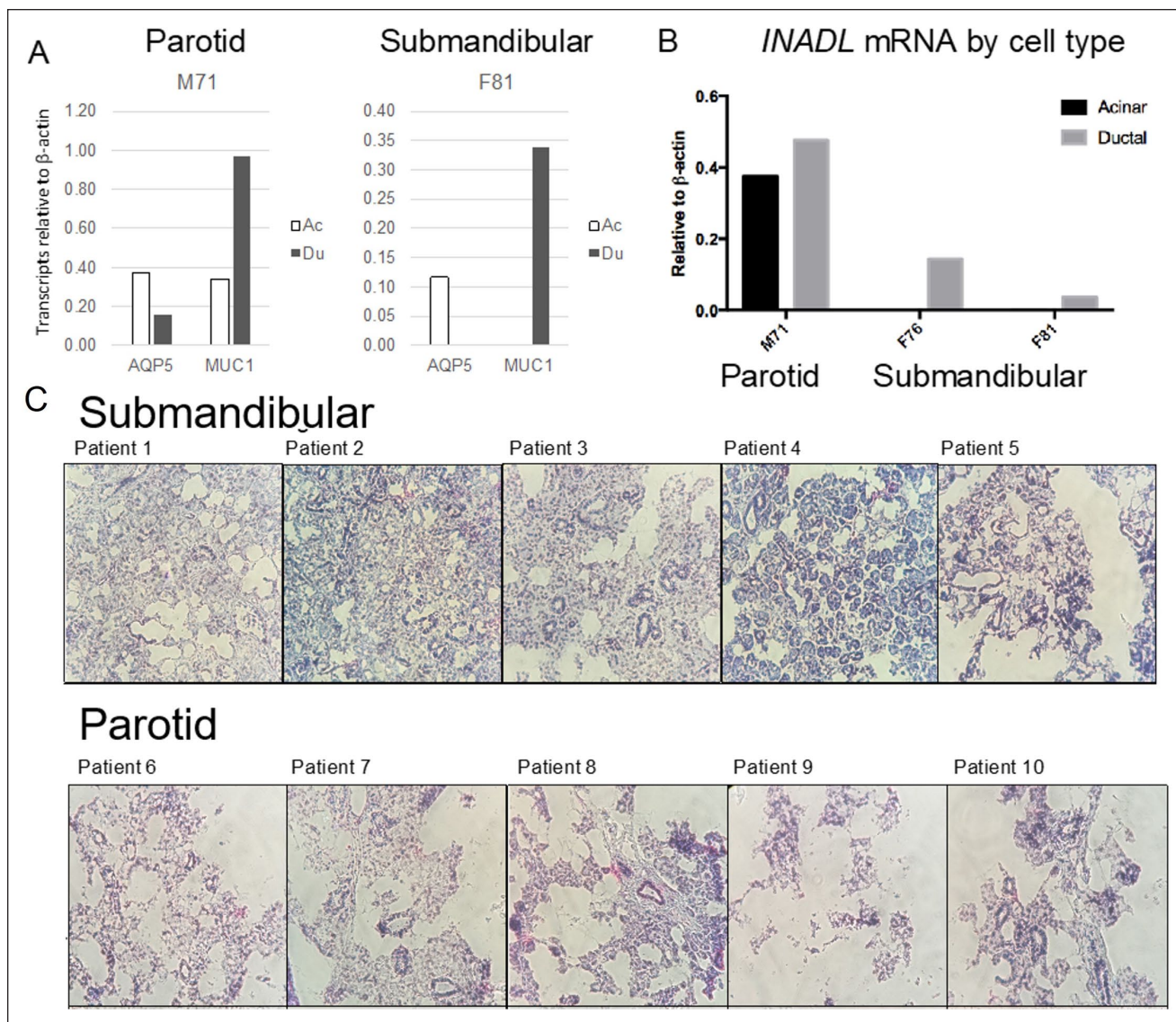
Figure 3. Enrichment of *INADL* and *MUC1* in ductal tissues. Parotid and submandibular frozen tissue sections were separated visually by laser capture microscopy (LCM) into acinar/myoepithelial and ductal fractions and prepared for quantitative polymerase chain reaction (qPCR) assessment of transcript expression (**A, B**). Note that submandibular tissue architecture was preserved, whereas parotid tissue structure was compromised by freezing (bottom panels visualized by U6 in situ hybridization), leading to more "compartment mixing" during laser capture (**C**). *INADL, MUC1*, and *AQ5* transcripts were examined for 1 parotid patient sample and 2 submandibular patient samples. *INADL* and *MUC1* were enriched in the ductal isolation, particularly for the submandibular samples. *AQ5* marked the acinar population. *INADL* was not detected in the "clean" acinar isolation from the submandibular gland but was detected by qPCR in dissected ducts in both submandibular patient samples.

served as controls of fraction purity. *INADL/PATJ, MUC1*, and *AQ5* transcripts were examined for 1 parotid patient sample and 2 submandibular patient samples, with only submandibular fractions passing quality control (Fig. 3A, right). In clean submandibular fractions, *INADL/PATJ* and *MUC1* were enriched in ductal isolates (Fig. 3A, B). No *AQ5* was detected in this fraction, indicating it was free from acinar cells. Thus, it appears that both INADL/PATJ and MUC1 are generally restricted to ductal cell populations in submandibular gland tissues. SCRIB was not assessed by this method.

SCRIB and INADL *Expression Precedes K19 Expression in Early Ductal-Differentiating hS/PCs*

We next determined if SCRIB or *INADL* expression could provide an earlier marker for cells initiating ductal differentiation than K19, the typical mature ductal marker. hS/PCs were encapsulated as single cells in hydrogels without acinar differentiation protocols (Srinivasan et al. 2017). Marker expression was assessed over 9 d. As seen in Figure 4 and Appendix Figure 5, cells assembled into multicellular spheroids of various sizes,
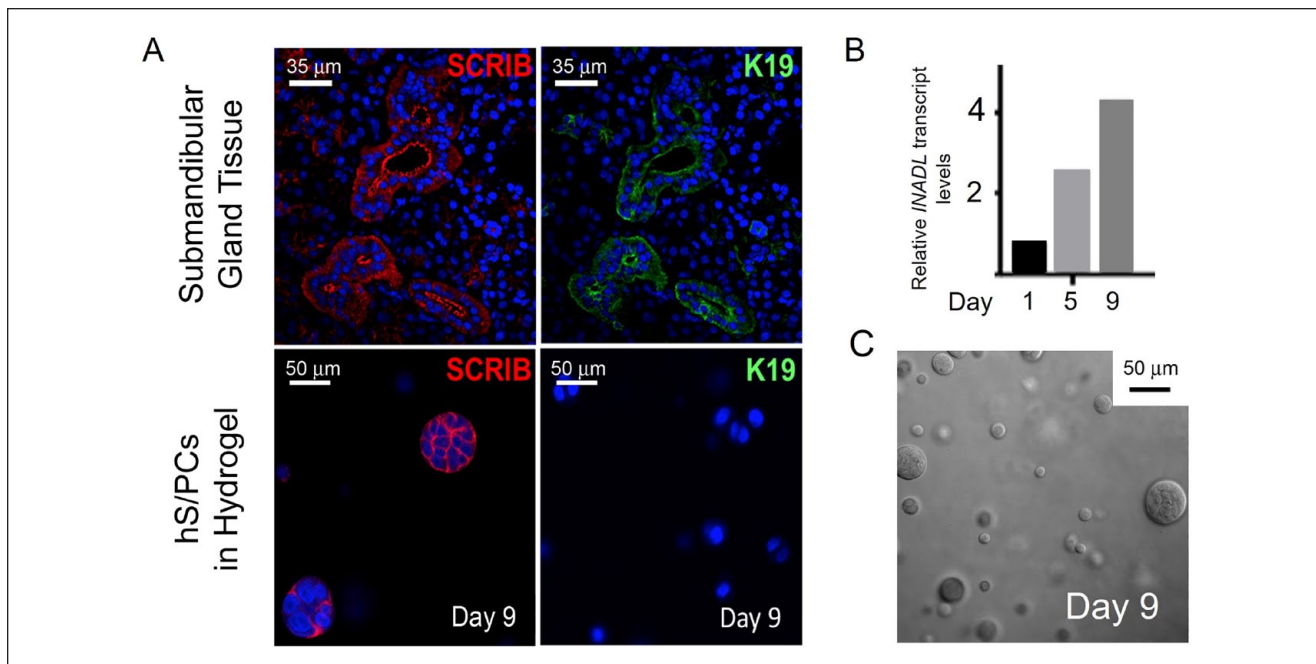
Figure 4. SCRIB and *INADL* expression precedes K19 expression in hyaluronic acid (HA) hydrogel encapsulated E-cadherin[+] (E-cad) human stem/progenitor cells (hS/PCs). (**A**) A comparison of human salivary tissue and 9-d encapsulated hS/PCs in hydrogel without acinar induction (see text). By day 9, hS/PC spheroids expressed SCRIB but did not express K19. (**B**) *INADL* transcripts increased over days 5 to 9 in spheroids in the absence of K19 expression. An increase in *INADL* transcript levels in Ecad[+] hS/PCs in HA hydrogels was observed. β-Actin served as the reference gene. (**C**) Assembling hS/PCs in hydrogel after 9 d are nonuniform in size, with the largest approximately 50 μm.
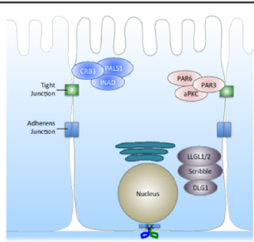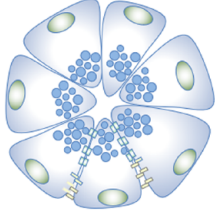
ranging from still single cells to structures containing 2 to 25 cells (Fig. 4C). Whereas in tissue, SCRIB and K19 were coexpressed in the same regions of ductal cells (Fig. 4A, upper), in assembling microstructures, SCRIB expression clearly preceded expression of K19 (Fig. 4A, lower). Apical MUC1 was not detected in encapsulated cells until they fully polarized and formed a lumen later in culture (not shown). *INADL* transcripts rose in clusters over the 9-d culture period in the absence of K19 staining (Fig. 4B). Assembling hS/PCs expressed both K5 and K14 (Appendix Fig. 5E, F) at the time they expressed SCRIB and β-catenin at the lateral surfaces (Fig. 4C), including in 2 cell couplets. The SCRIB-containing basolateral complex appears to assemble prior to the partition complex that remains diffuse at this stage. Together, these data indicate that polarity markers SCRIB and *INADL* can detect hS/PCs entering ductal differentiation and that K19 and MUC1 demarcate more mature ductal cells.

Discussion

Cell-based tissue engineering strategies to replace damaged/lost salivary tissue and restore function rely on fidelity of lineage differentiation of stem/progenitor cells. We examined pluripotency in epithelial lineages descended from hS/PCs to determine if early markers of cell adhesion or polarity could distinguish differentiating saliva-producing acinar and saliva-transporting ductal cells. We did not examine myoepithelial cells, as their origins/morphogenesis are complex (Gervais

et al. 2016; Ozdemir et al. 2017); we note that hS/PCs isolated without serum do not express αSMA and are morphologically dissimilar to primary myoepithelial cells isolated previously (Ozdemir et al. 2017). The study period we chose represents early epithelial differentiation before lumen formation and branching morphogenesis as occurs with addition of FGF 7/10 (Barrows et al. 2020). We earlier studied influences fostering acinar differentiation (Srinivasan et al. 2017); here we focused on identification of new markers for ductal progenitors. The ability to generate ductal structures in replacement tissues is essential for acinar secretory products to reach the oral cavity. Without ducts, implants could form intratissue cysts.

The keratin pair K5/14 is normally present in cells in the basal layer of stratified epithelia, and its expression decreases as basal stem/progenitor cells differentiate and lose proliferation potential (Alam et al. 2011). Similarly, p63 identifies a basal cell population in the salivary duct associated with tissue replenishment (Bilal et al. 2003; Song et al. 2018) and often is used to identify gland neoplasms (Bilal et al. 2003; Reis-Filho et al. 2003). Based on the coincidence of these 3 markers in salivary tissue at both protein and transcript levels (Appendix Figs. 2, 3, and 7) and their expression in our hS/PC population, we identified our pluripotent hS/PC population as a likely isolate of these basal cells. An excellent review (Weng et al. 2019) details the difficulty in identifying true stem cell populations in salivary tissues and suggests a need to further study p63-positive populations.

Classic Polarized Epithelial Model

- Integrin attachment confined to basal membrane

- Tight Junctions / Adherens Junctions provide lateral integrity

- Localized complexes (apical, partition, scribble) help establish apical-basal polarity

Modified from Iden and Collard. (2008) Nat Rev Mol Cell Biol. 9:846-859

Salivary Duct

- Cuboidal architecture

- Open lumen for fluid transport

- Early markers INADL, SCRIB

- Mature markers K19, apical MUC1

Salivary Acinus

- Pyramidal

- Irregular canalicular lumen

- Early markers diffuse α-amylase, MIST [*Srinivasan et al. 2017*]

- Mature marker apical α-amylase, nuclear MIST

Figure 5. Schematic comparing salivary acinar and ductal cells to a classical model of polarized epithelial cells. While salivary ductal cells represent the classical polarized cell model, acinar cells do not. These differences can be used to identify progenitor cell lineages in culture and acinar and ductal regions in tissues.

While both parotid and submandibular glands provide a ready source of hS/PCs, the tissues are different in terms of handling and processing for analysis. Frozen tissue quality from submandibular glands is superior for applications like laser capture microdissection, as its mucinous nature preserves its integrity, whereas serous parotid tissue is prone to peel apart. Both tissues perform well when frozen in OCT and fixed in PFA prior to immunostaining.

Most established lineage markers for salivary gland tissues are transcription factors, secretory products, aquaporins, or cytokeratins (Srinivasan et al. 2017; Sui et al. 2020). We identified new markers of ductal differentiation and validated their presence in primary human salivary tissue. Given their unique architectures and luminal surface area, acinar and ductal cells could possess different versions of the Crumbs, Partition, and Scribble/SCRIB polarity complexes. Because epithelial cells must polarize to form a lumen, we reasoned that components of polarity complexes might form early in differentiation, letting us distinguish acinar and ductal cells in early polarization. We examined several cell adhesion and polarity complexes to trace the emergence of these cell subpopulations. Immunostaining revealed that while cell adhesion molecules E-cadherin and

ZO-1 were present in both acinar and ductal regions, shape patterns were different with ducts in cross section in classical circular form with E-cadherin at the lateral junctions. Tight junctional ZO-1 staining revealed a recognizable pattern in acini that resembles "chicken feet," a structure that could assist the acinus with expansion and contraction during saliva secretion into the lumen (McManaman et al. 2006). Because complex structures are present in mature tissues but not in early differentiating cell lineages, they are not particularly useful for distinguishing early differences in mixtures of preacinar and preductal cells. Likewise, MUC1, established here and earlier (Gendler 2001) to demarcate fully polarized epithelial cells, is expressed late after lumen formation and is not useful to detect early events. It is, however, an excellent marker to identify ductal structures in salivary tissues.

Partition complex PAR3 was present in both acinar and ductal tissues and thus cannot identify emergent ductal structures. Fortunately, 2 other polarity complex constituents, SCRIB (basolateral scribble complex) and *INADL/PATJ* (apical complex), are present at high levels in ductal cells and absent or expressed at low levels in acinar structures. This finding makes each of these useful new markers for

identifying differentiating ductal cells in hS/PC cultures. In particular, SCRIB is ideal for immunostaining applications. *INADL/PATJ* is useful when transcript levels are assessed, but until a good, specific human antibody is available, it is limited for protein-based applications. Both SCRIB and *INADL/PATJ* are expressed in emergent ductal microstructures in 3-dimensional hydrogels before ductal marker K19, which we earlier found to require addition of branching-inducing growth factors FGF 7/10 (Barrows et al. 2020), not added to these cultures. Work in our (Srinivasan et al. 2017) and other (Nam et al. 2019) labs is actively examining use of defined extracellular matrices and growth factor combinations to direct cell differentiation along with neurotransmitters that affect branching morphogenesis. In future work, it will be useful to assess both SCRIB and INADL under conditions that promote both acinar and ductal differentiation during large-scale branching morphogenesis.

Based on this work and literature (Porcheri and Mitsiadis 2019), we propose a model in Figure 5 that distinguishes the architecture and components of polarity complexes in acinar and ductal cells in salivary glands and tissue-engineered correlates. While cuboidal ductal cells have distinct luminal, lateral, and basal sides that create a clear lumen for fluid transport, the pyramidal acinar cells have irregular lumens that can expand and contract like an accordion during saliva production. These distinct structures permit the two to be readily distinguished in tissue and can identify emergent acinar and ductal lineages during hS/PC differentiation in engineered tissue for cell-based therapies to restore salivation. We conclude that polarity markers SCRIB and INADL/PATJ are new early markers that identify progenitor cells entering a ductal path, while MUC1 is an excellent marker for identifying the lumen of mature ductal structures.

Author Contributions

D. Wu, contributed to conception, design, data acquisition, analysis, and interpretation, drafted and critically revised the manuscript; P.J. Chapela, contributed to conception, design, data acquisition, analysis, and interpretation, drafted the manuscript; C.M.L. Barrows, contributed to data acquisition, analysis, and interpretation, critically revised the manuscript; D.A. Harrington, contributed to conception, design, data analysis and interpretation, critically revised the manuscript; D.D. Carson, contributed to design, data analysis, and interpretation, critically revised the manuscript; R.L. Witt, contributed to conception and data acquisition, critically revised the manuscript; N.G. Mohyuddin, contributed to data acquisition, critically revised the manuscript; S. Pradhan-Bhatt, contributed to conception and data acquisition, critically revised the manuscript; M.C. Farach-Carson, contributed to conception, design, data analysis and interpretation, drafted and critically revised the manuscript. All authors gave final approval and agree to be accountable for all aspects of the work.

Acknowledgments

Declaration of Conflicting Interests

Funding

ORCID iDs

C.M.L. Barrows [iD] https://orcid.org/0000-0003-4696-9354

M.C. Farach-Carson [iD] https://orcid.org/0000-0002-4526-3088

References

Agostini BA, Cericato GO, Silveira ERD, Nascimento GG, Costa FDS, Thomson WM, Demarco FF. 2018. How common is dry mouth? Systematic review and meta-regression analysis of prevalence estimates. Braz Dent J. 29(6):606–618.

Alam H, Sehgal L, Kundu ST, Dalal SN, Vaidya MM. 2011. Novel function of keratins 5 and 14 in proliferation and differentiation of stratified epithelial cells. Mol Biol Cell. 22(21):4068–4078.

Assemat E, Bazellieres E, Pallesi-Pocachard E, Le Bivic A, Massey-Harroche D. 2008. Polarity complex proteins. Biochim Biophys Acta. 1778(3):614–630.

Barrows CML, Wu D, Farach-Carson MC, Young S. 2020. Building a functional salivary gland for cell-based therapy: more than secretory epithelial acini. Tissue Eng Part A. 26(23–24):1332–1348.

Bilal H, Handra-Luca A, Bertrand JC, Fouret PJ. 2003. P63 is expressed in basal and myoepithelial cells of human normal and tumor salivary gland tissues. J Histochem Cytochem. 51(2):133–139.

Bundgaard M, Moller M, Poulsen JH. 1977. Localization of sodium pump sites in cat salivary glands. J Physiol. 273(1):339–353.

Dirix P, Nuyts S, Van den Bogaert W. 2006. Radiation-induced xerostomia in patients with head and neck cancer: a literature review. Cancer. 107(11):2525–2534.

Gendler SJ. 2001. Muc1, the renaissance molecule. J Mammary Gland Biol Neoplasia. 6(3):339–353.

Gervais EM, Sequeira SJ, Wang W, Abraham S, Kim JH, Leonard D, DeSantis KA, Larsen M. 2016. Par-1b is required for morphogenesis and differentiation of myoepithelial cells during salivary gland development. Organogenesis. 12(4):194–216.

Kawamoto T, Nihei K, Nakajima Y, Kito S, Sasai K, Karasawa K. 2018. Comparison of xerostomia incidence after three-dimensional conformal radiation therapy and contralateral superficial lobe parotid-sparing intensity-modulated radiotherapy for oropharyngeal and hypopharyngeal cancer. Auris Nasus Larynx. 45(5):1073–1079.

Lee MG, Ohana E, Park HW, Yang D, Muallem S. 2012. Molecular mechanism of pancreatic and salivary gland fluid and HCO3 secretion. Physiol Rev. 92(1):39–74.

Martinez JR. 1987. Ion transport and water movement. J Dental Res. 66 Spec No:638–647.

Masedunskas A, Sramkova M, Weigert R. 2011. Homeostasis of the apical plasma membrane during regulated exocytosis in the salivary glands of live rodents. Bioarchitecture. 1(5):225–229.

Matsuzaki T, Ablimit A, Suzuki T, Aoki T, Hagiwara H, Takata K. 2006. Changes of aquaporin 5-distribution during release and reaccumulation of secretory granules in isoproterenol-treated mouse parotid gland. J Electron Microsc. 55(3):183–189.

McManaman JL, Reyland ME, Thrower EC. 2006. Secretion and fluid transport mechanisms in the mammary gland: comparisons with the exocrine pancreas and the salivary gland. J Mammary Gland Biol Neoplasia. 11(3–4):249–268.

Mitani H, Murase N, Mori M. 1989. Immunohistochemical demonstration of lysozyme and lactoferrin in salivary pleomorphic adenomas. Virchows Arch B Cell Pathol Incl Mol Pathol. 57(4):257–265.

Mortazavi H, Baharvand M, Movahhedian A, Mohammadi M, Khodadoustan A. 2014. Xerostomia due to systemic disease: a review of 20 conditions and mechanisms. Ann Med Health Sci Res. 4(4):503–510.

Nam K, Dean SM, Brown CT, Smith RJ Jr, Lei P, Andreadis ST, Baker OJ. 2019. Synergistic effects of laminin-1 peptides, VEGF and FGF9 on salivary gland regeneration. Acta Biomater. 91:186–194.

Ozdemir T, Srinivasan PP, Zakheim DR, Harrington DA, Witt RL, Farach-Carson MC, Jia X, Pradhan-Bhatt S. 2017. Bottom-up assembly of salivary gland microtissues for assessing myoepithelial cell function. Biomaterials. 142:124–135.

Pinna R, Campus G, Cumbo E, Mura I, Milia E. 2015. Xerostomia induced by radiotherapy: an overview of the physiopathology, clinical evidence, and management of the oral damage. Ther Clin Risk Manag. 11:171–188.

Porcheri C, Mitsiadis TA. 2019. Physiology, pathology and regeneration of salivary glands. Cells. 8(9):976.

Pradhan S, Zhang C, Jia X, Carson DD, Witt R, Farach-Carson MC. 2009. Perlecan domain IV peptide stimulates salivary gland cell assembly in vitro. Tissue Eng Part A. 15(11):3309–3320.

Proctor GB. 2016. The physiology of salivary secretion. Periodontol 2000. 70(1):11–25.

Reis-Filho JS, Simpson PT, Martins A, Preto A, Gartner F, Schmitt FC. 2003. Distribution of p63, cytokeratins 5/6 and cytokeratin 14 in 51 normal and 400 neoplastic human tissue samples using TARP-4 multi-tumor tissue microarray. Virchows Arch. 443(2):122–132.

Rodriguez-Boulan E, Macara IG. 2014. Organization and execution of the epithelial polarity programme. Nat Rev Mol Cell Biol. 15(4):225–242.

Schubert MM, Izutsu KT. 1987. Iatrogenic causes of salivary gland dysfunction. J Dent Res. 66 Spec No:680–688.

Song EC, Min S, Oyelakin A, Smalley K, Bard JE, Liao L, Xu J, Romano RA. 2018. Genetic and scRNA-seq analysis reveals distinct cell populations that contribute to salivary gland development and maintenance. Sci Rep. 8(1):14043.

Srinivasan PP, Patel VN, Liu S, Harrington DA, Hoffman MP, Jia X, Witt RL, Farach-Carson MC, Pradhan-Bhatt S. 2017. Primary salivary human stem/progenitor cells undergo microenvironment-driven acinar-like differentiation in hyaluronate hydrogel culture. Stem Cells Transl Med. 6(1):110–120.

Sui Y, Zhang S, Li Y, Zhang X, Hu W, Feng Y, Xiong J, Zhang Y, Wei S. 2020. Generation of functional salivary gland tissue from human submandibular gland stem/progenitor cells. Stem Cell Res Ther. 11(1):127.

Sullivan CA, Haddad RI, Tishler RB, Mahadevan A, Krane JF. 2005. Chemoradiation-induced cell loss in human submandibular glands. Laryngoscope. 115(6):958–964.

Vissink A, Panders AK, Gravenmade EJ, Vermey A. 1988. The causes and consequences of hyposalivation. Ear Nose Throat J. 67(3):166–168, 173–166.

Weng PL, Aure MH, Ovitt CE. 2019. Concise review: a critical evaluation of criteria used to define salivary gland stem cells. Stem Cells. 37(9):1144–1150.

Wu D, Chapela P, Farach-Carson MC. 2018. Reassembly of functional human stem/progenitor cells in 3D culture. Methods Mol Biol. 1817:19–32.

Wu D, Witt RL, Harrington DA, Farach-Carson MC. 2019. Dynamic assembly of human salivary stem/progenitor microstructures requires coordinated $\alpha 1\beta 1$ integrin-mediated motility. Front Cell Dev Biol. 7:224.